



# Effect of Iron Content on Crystallization and Microstructure of EN AC-42000 Alloy

T. Matuła \* , G. Siwiec , J. Piątkowski

Silesian University of Technology, Faculty of Materials Engineering,  
Kraśnińskiego 8, 40-019 Katowice, Poland

\* Corresponding author: E-mail address: tomasz.matula@polsl.pl

Received 20.11.2024; accepted in revised form 15.01.2025; available online 17.04.2025

## Abstract

The paper presents research on evaluating the crystallization of Al-Si alloys with increased iron content and analysis of the associated phase transformations. This problem is significant with the growing importance of recycling aluminum alloys, which is justified economically and ecologically. The study concerns the cooling curves of EN AC-42000 alloy (EN AC-AlSi7Mg), into which iron (in the form of Al-Fe mortar - as a substitute for circulating scrap) was introduced with a content of 0.5 to 1.5wt.%. Analysis of crystallization by ATD and microstructure studies of eleven Al-Si-Mg alloys with varying iron content showed up to about 0.4 wt.% Fe, the iron phases formed do not significantly affect the microstructure. They enter into multiphase eutectics of the type  $\alpha(\text{Al})+(\text{Mg}_2\text{Si,Fe})+\beta(\text{Si})$  or  $\alpha(\text{Al})+(\text{Al}_x\text{Fe}_y\text{Si}_z)+\beta(\text{Si})$ , which crystallize after the formation of the double eutectic  $\alpha(\text{Al})+\beta(\text{Si})$ . In the range of about 0.5 to 0.9 wt.% Fe, there is a preneutic crystallization of iron phases, mainly the lamellar-neutectic  $\beta\text{-Al}_5\text{FeSi}$ . At more than 1.0 wt.% Fe, the morphology of this phase becomes even more unfavorable (due to primary crystallization) and is accompanied by numerous clusters of shrinkage porosity.

**Keywords:** Cast aluminum alloys, Iron phases, Microstructure, Shrinkage porosity

## 1. Introduction

Studies [1, 2] show that the worst contaminant in Al-Si foundry alloys is iron, which most often crystallizes in the form of four phases with different morphologies [3, 4]:

1.  $\beta\text{-Al}_5\text{FeSi}$ , also referred to as  $\text{Al}_9\text{Fe}_2\text{Si}$  in Group 6XX.X (Al-Mg-Si) alloys [5],
2.  $\alpha\text{-Al}_8\text{Fe}_2\text{Si}$  (possibly  $\alpha\text{-Al}_{12}\text{Fe}_3\text{Si}_2$ ), which have a hexagonal structure under thermodynamic equilibrium conditions and are stable only in Al-Si-Fe alloys with very high purity of the feedstock components [6],
3.  $\delta\text{-Al}_4\text{FeSi}_2$  present in Al-Si alloys with more than 18wt.% Si,
4.  $\gamma\text{-Al}_3\text{FeSi}$  present at contents of more than 4wt.% Fe and more than 16wt.% Si [7].

Their morphology depends on crystallization conditions and chemical composition, but the  $\beta\text{-Al}_5\text{FeSi}$  ( $\beta\text{-Fe}$ ) phase is the worst. In Al-Si alloys with up to about 0.4wt.% Fe, this phase is not very harmful, as it crystallizes after the formation of dendrites of  $\alpha(\text{Al})$  solid solution and  $\alpha(\text{Al})+\beta(\text{Si})$  eutectic. In Al-Si alloys with magnesium additions, except for the  $\text{Mg}_2\text{Si}$  phase, there is a high probability of crystallization of the  $\text{Al}_9\text{Fe}_2\text{Si}$  phase with a single-stranded structure and the hexagonal  $\text{Al}_8\text{FeMg}_3\text{Si}_2$  phase. In addition, under conditions of thermodynamic imbalance, metastable phases  $\beta\text{-Al}_4\text{FeSi}$  (25.4wt.% Fe and 25.5wt.% Si) and  $\beta\text{-Al}_3\text{FeSi}$  (33.9wt.% Fe and 16.9wt.% Si) are formed [8]. In Al-Si-Cu(Fe) alloys, in addition to  $\text{Al}_2\text{Cu}$ , phases crystallized include:  $\text{Al}_6\text{FeCu}$  and  $\text{Al}_7\text{FeCu}_2$  entering into eutectics of the type  $\alpha(\text{Al})+\text{Al}_x\text{Fe}_y\text{Cu}_z+\beta(\text{Si})$  [9, 10].

However, the problem arises when the iron content of Al-Si alloys exceeds 0.4 % wt. (for gravity castings). Then, the



literature [11, 12] reports that the  $\beta$ -Al<sub>5</sub>FeSi phase crystallizes in a lamellar form, needle-like, on the surface of the deposit. Such a structure causes the propagation of microcracks and stress concentration, which increases the brittleness of castings, makes them more difficult to machine, and reduces their mechanical properties.

Therefore, it seems reasonable to undertake research on evaluating the crystallization of Al-Si alloys with higher iron content and analyzing the phase transformations involved. This problem is particularly relevant as the recycling of aluminum alloys becomes more important and economically and environmentally sound.

## 2. Purpose and scope of the study

The study's purpose was to analyze the crystallization process of EN AC-AlSi7Mg alloy with an increasing Fe content from 0.5 to 1.5 wt.%.

To achieve the stated purpose of the work, the scope of the research included:

- analysis of crystallization by ATD of EN AC-AlSi7Mg alloy with different iron content,
- evaluation of microstructure changes of AlSi7Mg alloy.

## 3. Material and research methodology

The test material was an EN AC-42000 (EN AC-AlSi7Mg) alloy, to which AlFe (20wt.%Fe and 80wt.%Al) master alloy (as a substitute for scrap iron) was added in such a quantity as to obtain the assumed content of 0.5 to 1.5wt.% Fe.

The alloys were melted in an electric resistance furnace PT12/100-PCH and, after reaching a temperature of about 760 °C,

were cast into a standard QC-4080 Heraeus Electro-Nite sampler with a capacity of 130 cm<sup>3</sup>. The solidification temperature (T) was recorded with a NiCr-NiAl thermocouple (type K) placed on the axis of the sampler. Thermal analysis was carried out with a Crystaldigraph NT3-8K temperature logger, using the MLab computer program. The transducer meets the requirements of both EN61010 and EN60584 for temperature measurement. The cooling curve  $T = f(\tau)$  and its first derivative after time  $dT/d\tau = f'(\tau)$  were recorded. For each recording of the cooling curve, equal "smoothing" factors and similar casting conditions were used.

The chemical composition of castings from QC-4080 samples was measured on the surface of castings on a Foundry Master CCD 01 L00113WAS-AG emission spectrometer (SpectroLab, Kleve, Germany). Ten samples each were made, discarding the two outliers, and the arithmetic mean was determined from the remaining eight samples.

Samples were cut from the thermal center of the QC-4080 sampler for metallographic examination. The specimens were ground and polished with polishing pastes of appropriate granularity, then etched in 1% HF acid. Ten metallographic images were taken each, of which those shown are representative images of the microstructure of EN AC-AlSi7Mg alloy.

Metallographic studies were carried out on a MeF-2 Reichert light microscope. X-ray microanalysis was conducted on a Hitachi S-4200 scanning microscope coupled to an EDS energy dispersive X-ray spectrometer using a Thermo Noran (System Six) system with a SE and BSE detector.

## 4. Research results

Table 1 shows the chemical composition of EN AC-42000 (EN AC-AlSi7Mg) alloy samples.

Table 1.  
Results of the chemical composition of EN AC-AlSi7Mg alloy (Al - balance)<sup>1;2</sup>

Sample No.	Elemental content, % wt.									
	Si	Fe	Mg	Cu	Mn	Ni	Sn	Zn	Pb	Ti
0.	6.97	0.21	0.51	0.16	0.25	0.10	≤0.03	≤0.06	≤0.10	0.12
1.	6.94	0.49	0.55	0.18	0.28	0.09	≤0.01	≤0.08	≤0.11	0.12
2.	7.12	0.61	0.53	0.19	0.29	0.12	≤0.01	≤0.08	≤0.11	0.11
3.	6.93	0.71	0.54	0.17	0.32	0.13	≤0.01	≤0.09	≤0.10	0.13
4.	7.11	0.80	0.64	0.16	0.29	0.06	≤0.02	≤0.11	≤0.09	0.13
5.	7.02	0.91	0.52	0.11	0.31	0.09	≤0.03	≤0.06	≤0.10	0.12
6.	7.41	1.01	0.58	0.16	0.27	0.11	≤0.02	≤0.11	≤0.11	0.18
7.	6.95	1.09	0.61	0.17	0.24	0.11	≤0.02	≤0.09	≤0.10	0.17
8.	7.17	1.19	0.58	0.15	0.30	0.08	≤0.03	≤0.11	≤0.09	0.20
9.	7.26	1.28	0.52	0.16	0.30	0.08	≤0.02	≤0.07	≤0.10	0.15
10.	7.22	1.40	0.60	0.19	0.27	0.12	≤0.02	≤0.11	≤0.08	0.18
11.	6.98	1.51	0.57	0.17	0.28	0.13	≤0.02	≤0.11	≤0.06	0.18

<sup>1</sup> – averaged results from 6 measurements, after discarding the two outliers,

<sup>2</sup> – The sum of other elements (Na) and impurities (Ca; K) in the EN AC-AlSi7Mg alloy is below 0.10wt.%.

Analyzing the results of the chemical composition of the EN AC-AlSi7Mg alloy (Table 1), it can be concluded that despite the

increasing iron content, the proportion of other elements has not changed and is within the limits of the EN 1706:2010 standard.

## 4.1. ATD thermal analysis of AlSi7Mg alloy

Based on ATD thermal analysis studies, the cooling curve of EN AC-AlSi7Mg alloy is up to about 0.4wt.% Fe content was typical of that alloy (Fig.1). At contents from 0.5 to about 0.9wt.% Fe, an exothermic effect from crystallization of iron-rich phases was found. It occurs in the temperature range from about 585°C to about 600°C, which is before the crystallization of the  $\alpha(\text{Al})+\beta(\text{Si})$  eutectic (about 578°C) and the triple eutectic containing the  $\text{Mg}_2\text{Si}$  phase (about 550°C), whose crystallization lasts to the temperature of  $T_{\text{sol}}$ . (about 500°C). Increased iron content in the EN AC-AlSi7Mg alloy (more than 1.0wt.%) causes primary crystallization of the iron phases (before crystallization of the dendrites of solid solution  $\alpha$ ), accompanied by an exothermic effect above 600°C. Further increasing the proportion of iron causes an even greater increase in this temperature.

Representative ATD diagrams of EN AC-AlSi7Mg alloy with different iron contents are shown in Figure 2.

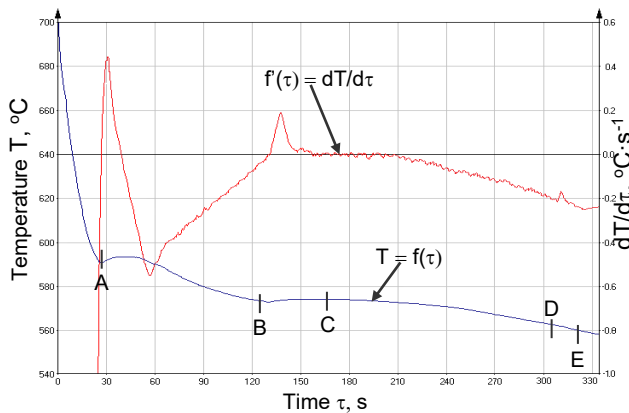


Fig. 1. ATD of EN AC-AlSi7Mg alloy with 0.2wt.% Fe

The symbols in Figures 1 to 2 stand for:

- $T=f(\tau)$  - the curve of temperature change  $T$  at time  $t$ , - the so-called TA (Temperature Analysis) curve,
- $dT/d\tau = f'(\tau)$  - the first derivative of the temperature change over time - the so-called ATD (Analysis Temperature Derivative) curve,
- point A - temperature of onset of crystallization of dendrites of solid solution  $\alpha(\text{Al})$  -  $T_{\alpha(\text{Al})}$  ( $T_{\text{liq}}$ ), °C,
- A-B - range of crystallization of dendrites of solid solution  $\alpha(\text{Al})$ , °C,
- point B - minimum temperature (onset) of crystallization of eutectic  $\alpha(\text{Al})+\beta(\text{Si})$ , -  $T_{\text{Emin}(\alpha+\beta)}$  °C,
- point C - average crystallization temperature of the  $\alpha(\text{Al})+\beta(\text{Si})$ , -  $T_{\text{E}(\alpha+\beta)}$  °C,
- point X - crystallization temperature of iron-rich intermetallic phases -  $T_{\text{E}(\text{Fe})}$ , °C,
- point D - crystallization temperature of magnesium-rich intermetallic phases -  $T_{\text{E}(\text{Mg})}$ , °C,
- point E - temperature of the end of crystallization of EN AC-AlSi7Mg alloy ( $T_{\text{sol}}$ ), °C.

Table 2.

Table 2 summarizes the average characteristic crystallization temperatures of EN AC-AlSi7Mg alloy obtained from the ATD method (rounded to integer) for different iron contents.

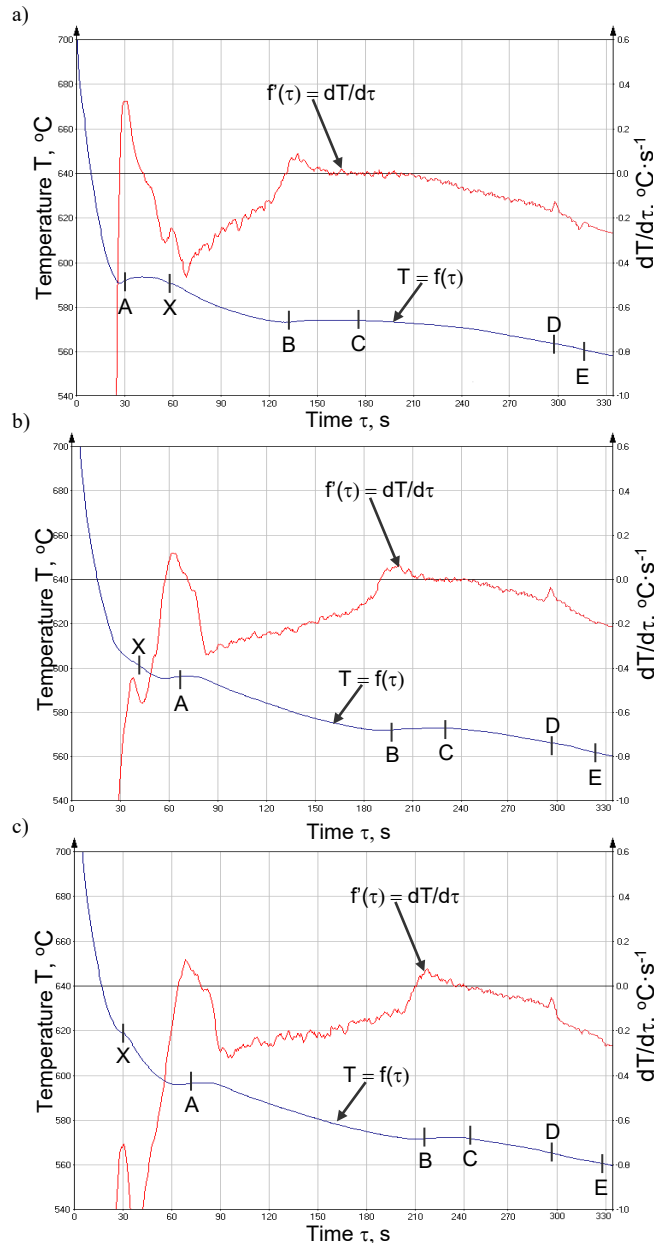


Fig. 2. ATD of EN AC-AlSi7Mg alloy with: a) 0.5 to 0.9wt.%; b) 1.0 to 1.4wt.%; c) above 1.4wt.% with characteristic temperatures

Characteristic crystallization temperatures of EN AC- $\text{AlSi7Mg}$  alloy read from ATD charts <sup>1</sup>

Sample No.	Name of alloy and share of iron, wt.%	Characteristic crystallization temperatures, °C					
		A $T_{\text{liq.}}$	B $T_{\text{Emin}(\alpha+\beta)}$	C $T_{\text{E}(\alpha+\beta)}$	X $T_{\text{E}(\text{Fe})}$	D $T_{\text{E}(\text{Mg})}$	E $T_{\text{sol.}}$
0.	$\text{AlSi7Mg}$	590	573	579	-----	562	558
1.	$\text{AlSi7Mg}+0.5$	595	575	578	585	566	551
2.	$\text{AlSi7Mg}+0.6$	598	576	577	587	562	552
3.	$\text{AlSi7Mg}+0.7$	598	575	577	591	563	558
4.	$\text{AlSi7Mg}+0.8$	599	576	578	597	564	555
5.	$\text{AlSi7Mg}+0.9$	599	574	579	600	567	551
6.	$\text{AlSi7Mg}+1.0$	600	576	577	600	562	555
7.	$\text{AlSi7Mg}+1.1$	601	576	578	604	564	559
8.	$\text{AlSi7Mg}+1.2$	599	575	578	609	567	553
9.	$\text{AlSi7Mg}+1.3$	600	576	579	610	562	552
10.	$\text{AlSi7Mg}+1.4$	600	574	578	616	565	555
11.	$\text{AlSi7Mg}+1.5$	600	575	577	620	567	552

<sup>1</sup> – the symbols in the table are the same as in Figure 2.

## 4.2. Results of microstructure tests

Examples of the EN AC- $\text{AlSi7Mg}$  alloy microstructures with different iron contents are shown in Figure 3.

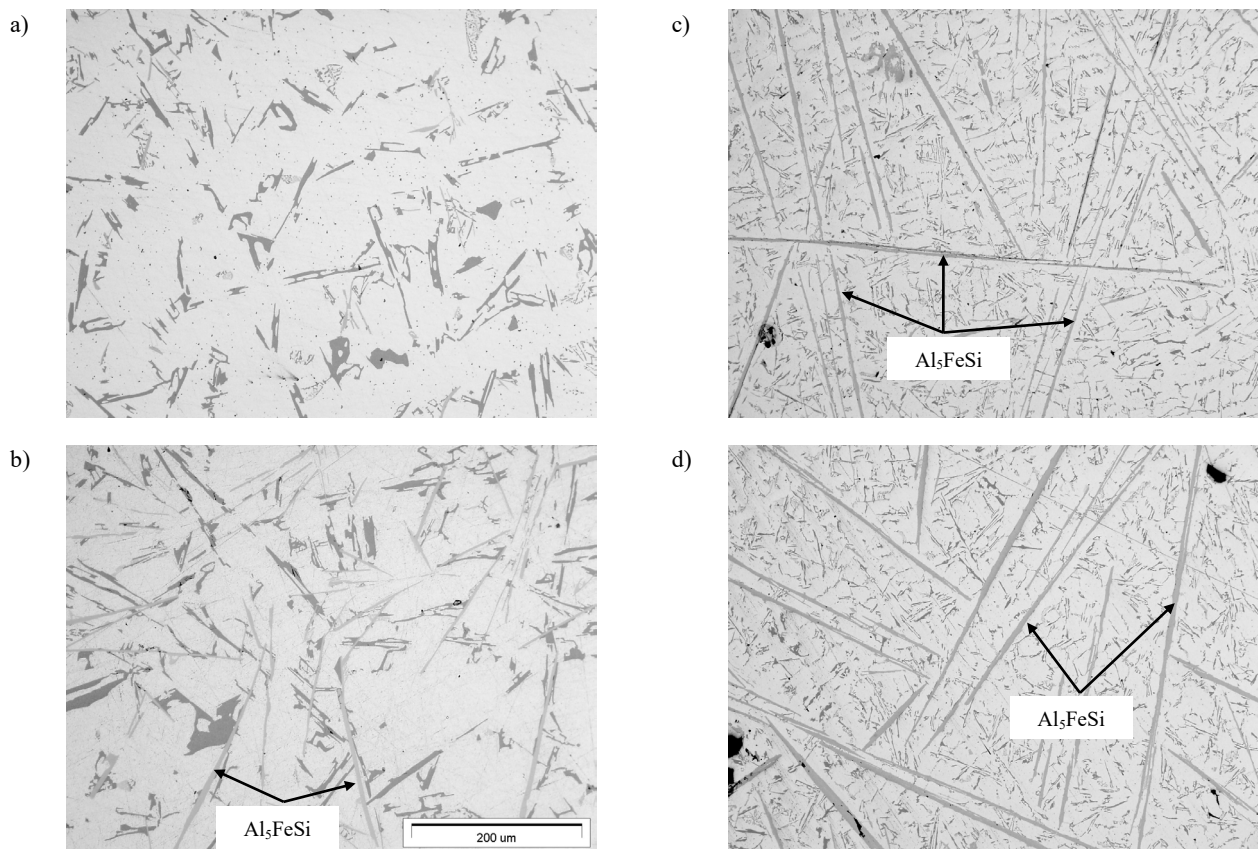


Fig. 3. Microstructure of EN AC- $\text{AlSi7Mg}$  alloy with iron content: a) to 0.2 b) from 0.21 to approx. 0.49; c) from 0.5 to 0.9; d) from 0.9 to 1.5 (wt.%)

EDS analyses, supported by XRD studies, show that in addition to diffraction lines originating from the solid solution of  $\alpha(\text{Al})$ , silicon crystals  $\beta(\text{Si})$ ,  $\text{Mg}_2\text{Si}$  phase, diffraction lines of iron phases (e.g.  $\text{Al}_8\text{Fe}_2\text{Si}$  and  $\text{Al}_{20}\text{Fe}_3\text{Si}_2$ ) were identified, however the most abundant phase was  $\beta\text{-Al}_5\text{FeSi}$ . The results of XRD studies were presented in the studies [13].

After exceeding approx. 0.45 wt.% Fe in the  $\text{AlSi7Mg}$  alloy, numerous porosities become visible around the  $\beta\text{-Al}_5\text{FeSi}$  phase precipitates (as the iron content increases), as shown in Figure 4.

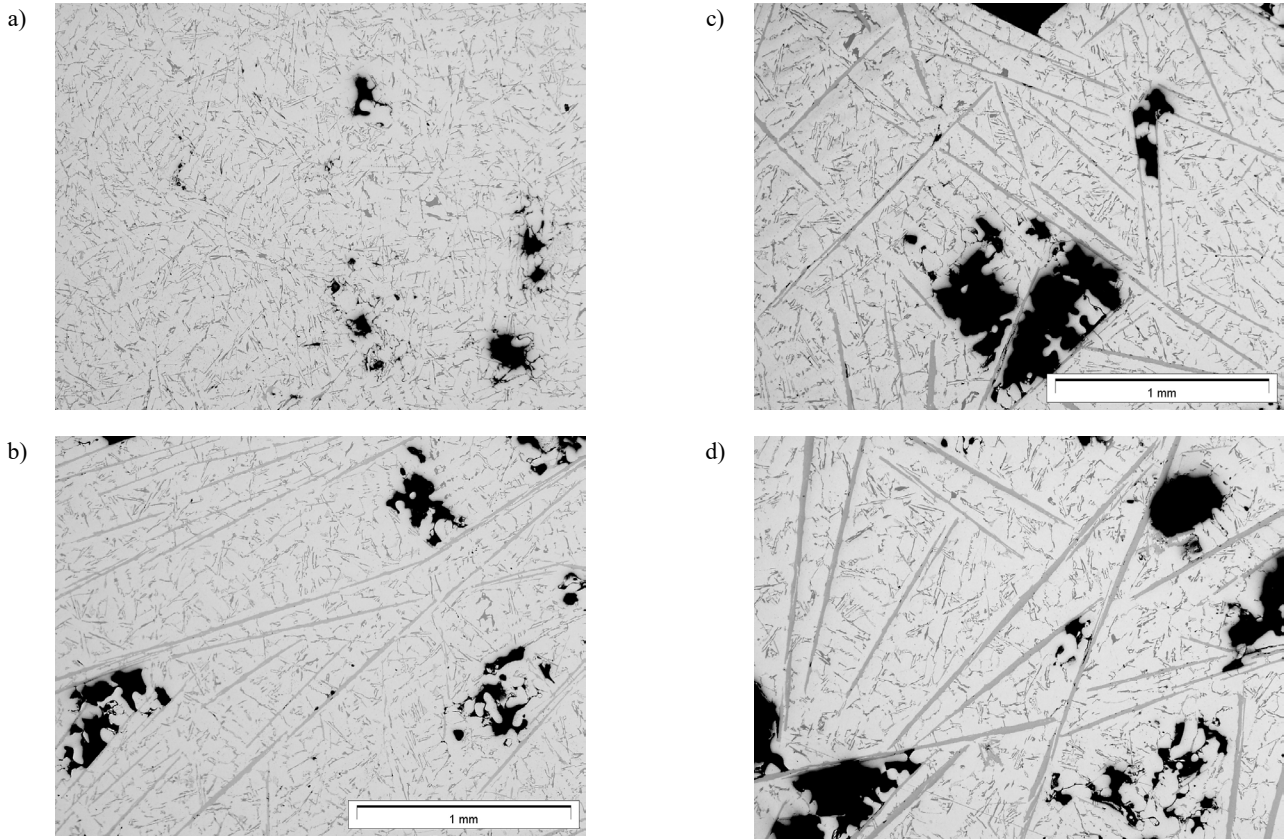


Fig. 4. Porosity between acicular precipitates of the  $\beta\text{-Al}_5\text{FeSi}$  phase in the EN AC-AlSi7Mg alloy with iron content: a) to 0.2 b) from 0.21 to approx. 0.49; c) from 0.5 to 0.9; d) from 0.9 to 1.5 (wt.%)

## 5. Analysis of research results

The ATD analysis shows the crystallization of the EN AC-AlSi7Mg alloy with a content of up to about 0.4wt.% proceeds traditionally for silumins with a hypoeutectic composition with magnesium content (up to 0.55wt.%). The primary crystallizing dendrites are the solid solution  $\alpha(\text{Al})$  in the temperature range from about 595 to 574°C. Then, the double eutectics  $\alpha(\text{Al})+\beta(\text{Si})$ , multicomponent eutectics of the type  $\alpha(\text{Al})+\text{Al}_x\text{Fe}_y\text{Si}_z+\beta(\text{Si})$  rich in iron and the triple eutectic  $\alpha(\text{Al})+\text{Mg}_2\text{Si}+\beta(\text{Si})$  nucleate. Their crystallization lasts until the temperature  $T_{\text{sol}}$  equal to about 500°C, which is also the end of the solidification of the EN AC-AlSi7Mg alloy (Table 2).

Increasing the iron content from 0.5 to about 0.9wt.% changes the crystallization order. ATD analyses, EDS and XRD studies show that after the formation of  $\alpha(\text{Al})$  dendrites, the  $\beta\text{-Al}_5\text{FeSi}$  phase crystallizes pre-eutectically (point X in Fig. 2 and Table 2).

The further course of crystallization of the EN AC-AlSi7Mg alloy is without significant changes.

At a content of over 0.90wt.% Fe, the cooling curve of the EN AC-AlSi7Mg alloy indicates that the  $\beta\text{-Al}_5\text{FeSi}$  phase crystallizes initially (at a temperature of over 600°C). Microstructure studies show that the morphology of the  $\beta\text{-Al}_5\text{FeSi}$  phase is plate-like (on the surface of the metallographic microsection – acicular).

Based on ATD studies, it can be concluded that the crystallization of the EN AC-AlSi7Mg alloy with an increasing share of iron proceeds in the following stages:

1. for the EN AC-AlSi7Mg alloy with a content of up to approx. 0.49wt.% Fe:
  - stage 1: start of the crystallization process of the dendrites of the solid solution  $\alpha(\text{Al})$  – temp.  $T_{\text{liq}}$ ,
  - stage 2: nucleation and crystallization of the double eutectic  $\alpha(\text{Al})+\beta(\text{Si})$  – temp.  $T_{\text{E}(\alpha+\beta)}$ ,
  - stage 3: nucleation and crystallization of multicomponent eutectics of the type

- $\alpha(\text{Al})+\text{Al}_x\text{Fe}_y\text{Si}_z+\beta(\text{Si})$  and triple  $\alpha(\text{Al})+\text{Mg}_2\text{Si}+\beta(\text{Si})$  – temp.  $T_{E(\text{Fe})}$  and  $T_{E(\text{Mg})}$ ,
- stage 4: end of the alloy crystallization process – temp.  $T_{\text{sol}}$ .
2. for the EN AC- $\text{AlSi7Mg}$  alloy with a content of approx. 0.5 to 0.9wt.% Fe:
    - stage 1: start of the crystallization process of the dendrites of the solid solution  $\alpha(\text{Al})$  – temp.  $T_{\text{liq}}$ ,
    - stage 2: nucleation and pro-eutectic crystallization of the  $\beta\text{-Al}_5\text{FeSi}$  phase – temp.  $T_{E(\text{Fe})}$ ,
    - stage 3: crystallization of the double eutectic  $\alpha(\text{Al})+\beta(\text{Si})$  and subsequent stages unchanged.
  3. for the EN AC- $\text{AlSi7Mg}$  alloy with a content of over 0.9% wt. Fe:
    - stage 1: nucleation and primary crystallization of the  $\beta\text{-Al}_5\text{FeSi}$  – temp.  $T_{E(\text{Fe})}$ ,
    - stage 2: crystallization of the  $\alpha(\text{Al})$  – temp dendrites.  $T_{\alpha(\text{Al})}$ ,
    - stage 3: crystallization of the double eutectic  $\alpha(\text{Al})+\beta(\text{Si})$  and subsequent stages unchanged.

Based on microscopic examinations, it can be stated that the EN AC- $\text{AlSi7Mg}$  alloy contains: dendrites of the solid solution  $\alpha(\text{Al})$  - the alloy matrix, silicon crystals  $\beta(\text{Si})$ , which are part of the double eutectic  $\alpha(\text{Al})+\beta(\text{Si})$ , the  $\text{Mg}_2\text{Si}$  phase - as a component of the triple eutectic  $\alpha(\text{Al})+\text{Mg}_2\text{Si}+\beta(\text{Si})$  and iron-rich phases, the most abundant of which is  $\beta\text{-Al}_5\text{FeSi}$  with a lamellar morphology (on the surface of the acicular microsection). The privileged direction of growth in one direction causes this phase (especially with a content of over 1.0wt.% Fe) to be often cracked longitudinally or transversely (Fig. 5).

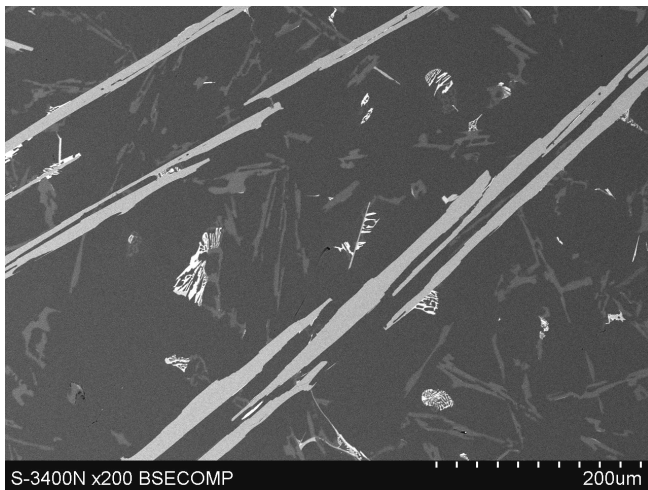


Fig. 5. SEM microstructure of the  $\text{AlSi7Mg}$  alloy containing  $\beta\text{-Al}_5\text{FeSi}$  phase cracks

Long precipitates of the  $\beta\text{-Al}_5\text{FeSi}$  phase (from 600  $\mu\text{m}$  to even 1000  $\mu\text{m}$ ) are also privileged places for the formation of porosity, as they reduce the interdendritic permeability, and therefore block (inhibit) the free flow of the liquid alloy during cooling. The moving crystallization front "does not keep up" with filling the places "closed" by the  $\beta\text{-Fe}$  phases with liquid metal,

causing the formation of shrinkage pores in the vicinity of the needles of the  $\beta\text{-Al}_5\text{FeSi}$  phases - Figure 3. The presence of voids causes local stresses, which during the work of the castings transform into micro- and macrocracks. This is because the needle-like precipitates of the  $\beta\text{-Fe}$  phases oriented with their longer side perpendicular to the given load undergo decohesion. At the same time, those arranged parallel - cracks along their arms and fragments.

It should, therefore, be assumed that the  $\beta\text{-Al}_5\text{FeSi}$  phases that appear in the microstructure of the EN AC- $\text{AlSi7Mg}$  alloy after exceeding approx. 0.45wt.% Fe constitutes the nuclei of pores and/or shrinkage micro shrinkages, increasing the porosity of the castings and reducing the feeding capacity by reducing the flow of liquid alloy between the branched dendrites of the  $\alpha(\text{Al})$  solid solution. They constitute the sites of initiation of microcracks, which reduce the alloys' strength, impact strength, and plasticity. The size of the  $\beta\text{-Al}_5\text{FeSi}$  intermetallic phase precipitates, especially their very unfavorable morphology, also makes the machining of castings difficult.

Based on ATD, microstructure, and literature review [2, 3, 5], it was found that the essential criterion determining the formation of a given type of iron phase is, among others, its content and the cooling rate of the alloy. Phases that crystallize before the formation of dendrites of the  $\alpha(\text{Al})$  solid solution, growing freely in the metallic liquid or those that are formed at the same time as the dendritic network (but in the remaining liquid), tend to grow much more ( $\beta\text{-Fe}$  phase) than those that are formed later - during or after the formation of eutectics.

## 6. Conclusions

Based on the conducted studies, the following conclusions were formulated:

1. In the  $\text{AlSi7Mg}$  alloy with a content of up to approx. 0.49wt.% Fe, the crystallizing iron phases are part of multicomponent eutectics with a small effect on the microstructure.
2. Increasing the iron content from 0.5 to approximately 0.9wt.% causes a change in the crystallization order of the  $\text{AlSi7Mg}$  alloy. The  $\beta\text{-Al}_5\text{FeSi}$  phase precipitates crystallize before the  $\beta\text{-Al}_5\text{FeSi}$  is eutectic. Their average length is approximately 500  $\mu\text{m}$  to 600  $\mu\text{m}$ .
3. At a content of over 0.9wt.% Fe, the  $\beta\text{-Al}_5\text{FeSi}$  phases crystallize primarily. Their average length is from 600  $\mu\text{m}$  to even 1000  $\mu\text{m}$ . Freely growing plate-acicular  $\beta\text{-Fe}$  phases block interdendritic channels, hinder the flow of liquid alloy, causing increased porosity of castings.
4. Content of over 0.90wt.% Fe also causes the  $\beta\text{-Al}_5\text{FeSi}$  phase precipitates to crack, which probably additionally affects the reduction of strength properties of  $\text{Al-Si(Fe)}$  alloys.

## Acknowledgments

This research was funded by the Silesian University of Technology, grant number 11/020/BK\_23/0104.

## References

- [1] MacKenzie, S.D., Totten, G.E. (2005). *Analytical characterization of aluminum, steel, and superalloys*. (1st ed.). Boca Raton: Taylor and Francis Group.
- [2] Xinjin, Cao, & Campbell, J. (2006). Morphology of  $\beta$ -Al<sub>5</sub>FeSi phase in Al-Si cast alloys. *Materials Transaction*. 47(5), 1303-1312. <https://doi.org/10.2320/matertrans.47.1303>.
- [3] Taylor, J.A. (2004). The effect of iron in Al-Si cast alloys. In 35th Australian Foundry Institute National Conference, 31 October - 3 November 2004 (pp. 148-157). Australia: Australian Foundry Institute.
- [4] Ebhota, W.S. Tien-Chien, J. (2018). Intermetallics formation and their effect on mechanical properties of Al-Si-X alloys. In Mahmood Aliofkhazraei (Eds.), *Intermetallic Compounds - Formation and Applications* (pp. 21-38). London, United Kingdom: IntechOpen.
- [5] Taylor, J.A. (2012). Iron-containing intermetallic phases in Al-Si based casting alloys. *Procedia Materials Science*. 1, 19-33. DOI: 10.1016/j.mspro.2012.06.004.
- [6] Zavadská, D., Tillova, E., Svesova, I., Chalupova, M., Kucharikova, L. & Belan, J. (2019). The effect of iron content on microstructure and porosity of secondary AlSi7Mg0.3 alloy. *Periodica Polytechnica Transportation Engineering*. 47(4), 283-289. <https://doi.org/10.3311/PPtr.12101>.
- [7] Orozco-Gonzales, P., Castro-Roman, M., Martinez, A.I., Herrero-Trejo, M., Lopez, A.A. & Quispe-Marcatoma, J. (2010). Precipitation of Fe-rich intermetallic phase in liquid Al-13.58Si-11.59Fe-1.19Mn alloy. *Intermetallics*. 18(8), 1617-1622. <https://doi.org/10.1016/j.intermet.2010.04.014>.
- [8] Belov, N.A., Aksenov, A.A. & Eskin, D.G. (2002). *Iron in aluminum alloys. Impurity and Alloying Element* (1st ed.). New York: Taylor & Francis Inc.
- [9] Liu, G., Gong, M., Xie, D. & Wang, J. (2019). Structures and mechanical properties of Al-Al<sub>2</sub>Cu interfaces. *The Journal of The Minerals, Metals & Materials Society*. 71, 1200-1208. DOI: 10.1007/s11837-019-03333.
- [10] Hurtalowa, L., Tillova, E. & Chalupova, M. (2012). Identification and analysis of intermetallic phases in age-hardened recycled AlSi9Cu3 alloy. *Archive of Mechanical Engineering*. LIX(4), 385-393. DOI: 10.2478/v10180-012-0020-3.
- [11] Lu, L. & Dahle, A.K. (2005). Iron-rich intermetallic phases and their role in casting defect formation in hypoeutectic Al-Si alloys. *Metallurgical and Mechanical Transactions*. 36A, 819-835. <https://doi.org/10.1007/s11661-005-1012-4>.
- [12] Xiao, F., Li, L., Zhou, R., Li, Y., Jiang, Y., Lu & D. (2018). Effect of melt treatment on Fe-rich phase in Al-25Si-2Fe-2Mn alloy. *Advances in Materials Processing*. 865-879. DOI: 10.1007/978-981-13-0107-0\_85.
- [13] Piątkowski, J. (2020). The crystallization of the AlSi9 alloy designed for the alfin processing of ring supports in engine pistons. *Archives of Foundry Engineering*. 20(2), 65-70. DOI 10.24425/afe.2020.131304.